JOURNAL OF PROPULSION AND POWER
Vol. 26, No. 4, July–August 2010

Engineering Model for Self-Pressurizing Saturated-N_2O-Propellant Feed Systems

Stephen A. Whitmore* and Spencer N. Chandler†
Utah State University, Logan, Utah 84322-4130

DOI: 10.2514/1.47131

Self-pressurizing propellant feed systems, due to their overall simplicity, offer attractive options for propulsion system designers. These systems inherently exhibit transient properties as the tank-fluid mass bleeds down, and modeling the two-phase blow-down or evacuation process using first-principle physics is an extremely complex and time-intensive problem. As an alternative, a simple engineering model is developed for self-pressurized saturated-propellant feed systems. The model assumes an adiabatic expansion for which, during evacuation, the current tank-fluid entropy and the fluid entropy that has escaped through the feed system equate to the initial tank-fluid entropy. Mass flow through the outlet orifice is modeled as a two-phase nonhomogeneous nonequilibrium process. The evacuated entropy is subtracted from the total entropy at the state of the fluid leaving the tank, then the new state with the existing mass and entropy is calculated using two-phase thermodynamic property tables. In this manner, the tank-fluid state is calculated continuously during the evacuation. This propellant feed-system evacuation model is developed using saturation fluid properties for nitrous oxide, but it is readily extensible to other saturated propellants. Model results are compared with data derived from cold-flow tests conducted on a small-scale hybrid rocket motor. The comparisons show excellent agreement.

Nomenclature

A_c	=	orifice cross-sectional area, cm^2
A_{out}	=	tank-outlet area, cm^2
A_{vent}	=	tank-vent area, cm^2
C_d	=	discharge coefficient
C_{dout}	=	tank-outlet discharge coefficient
C_{dvent}	=	tank-vent discharge coefficient
D	=	injector orifice diameter, cm
h_1	=	injector or orifice upstream specific enthalpy, kJ/kg
h_2	=	injector or orifice downstream specific enthalpy, kJ/kg
i	=	iteration time index
L	=	injector orifice length, cm
L/D	=	orifice aspect ratio
$\dot{m}_{HEM}$	=	mass-flow rate calculated using homogeneous equilibrium model formula, kg/s
$\dot{m}_{inc}$	=	mass-flow rate calculated using incompressible discharge coefficient formula, kg/s
m_L	=	liquid propellant mass, kg
$\dot{m}_{L,out}$	=	liquid mass-flow rate of propellant leaving the tank outlet, kg/s
$\dot{m}_{NHNE}$	=	mass-flow rate calculated using nonhomogeneous nonequilibrium model formula, kg/s
m_{total}	=	total fluid mass in tank
m_V	=	vapor propellant mass, kg
$\dot{m}_{V,out}$	=	vapor mass-flow rate of propellant leaving the tank outlet, kg/s
m_0	=	initial mass of fluid in tank, kg
P_{out}	=	tank outlet or rocket chamber pressure, kPa
P_v	=	fluid vapor pressure, kPa
P_0	=	initial tank fluid pressure, kPa
P_1	=	injector or orifice upstream pressure, kPa
P_2	=	injector or orifice downstream pressure, kPa
P_∞	=	ambient pressure, kPa
R_g	=	gas constant, kJ/kg · K
s	=	effective specific entropy, kJ/kg · K
s_L	=	specific entropy of the liquid propellant, kJ/kg · K
S_{total}	=	total entropy at state one, kJ/K
s_V	=	specific entropy of the vapor propellant, kJ/kg · K
S_0	=	initial total entropy, kJ/K
s_0	=	initial specific entropy, kJ/kg · K
T_0	=	initial tank-fluid temperature, K
t	=	time, s
V_L	=	tank volume occupied by liquid, m^3
V_{tank}	=	propellant tank volume, m^3
V_v	=	tank volume occupied by liquid, m^3
Z	=	compressibility factor
γ	=	ratio of specific heats
Δh	=	specific enthalpy change, m^2/s^2
Δm_L	=	liquid mass change, kg
Δm_V	=	vapor mass change, kg
Δt	=	time-step interval, s
κ	=	nonhomogeneous nonequilibrium model-weighting parameter
ρ	=	effective tank-propellant density, kg/s
ρ_L	=	liquid propellant density, kg/s
ρ_V	=	propellant vapor density, kg/s
ρ_0	=	initial total density of fluid in tank, kg/s
ρ_2	=	injector or orifice downstream total fluid density, kg/s
χ	=	quality of fluid mixture (vapor mass fraction)

Received 10 September 2009; revision received 21 February 2010; accepted for publication 23 February 2010.

*Assistant Professor, Mechanical and Aerospace Engineering, 4130 Old Main Hill. Associate Fellow AIAA.

†Graduate Research Assistant, Mechanical and Aerospace Engineering, 4130 Old Main Hill. Student Member AIAA.

I. Introduction

ROCKET engines with constant-pressure feed systems rely on complex turbomachinery or highly pressurized gas cylinders filled with inert gasses, like nitrogen or helium, and the associated pneumatic devices required to deliver propellant. These pressurizing systems add complexity and weight, always undesirable features for any flight system; but these features present critical disadvantages for small-scale systems, like sounding rockets or space thrusters. However, there exists a class of propellants, like nitrous oxide (N_2O), that are saturated at room temperature and possess high-saturation vapor pressures, greater than 6000 kPa at 300 K. These characteristics allow the propellant feed systems to self pressurize and avoid

the complexity of an electromechanical feed system. Rockets and thrusters that use self-pressurizing propellant feed systems, due to their inherent simplicity, offer attractive options for propulsion system designers.

Although self-pressurizing propellant feed systems offer significantly less mechanical complexity when compared with constant-pressure systems, their use presents significant modeling challenges. Self-pressurizing feed systems inherently exhibit transient fluid properties during the propellant tank evacuation, and modeling the process using first-principle physics, such as computational fluid dynamics (CFD), is an extremely complex and time-intensive problem. As an alternative to two-phase CFD calculations, a simple engineering model for self-pressurized feed systems that use saturated compressible propellants is developed and evaluated in this paper.

The engineering model presented here uses the saturation fluid properties for N_2O, but it is readily extensible to other saturated propellants. Although the authors recognize that N_2O has only average oxidizer-performance characteristics, this propellant is used here for three key reasons: 1) N_2O has low toxicity and relatively safe handling properties, 2) N_2O has a high vapor pressure at room temperature, giving it ideal self-pressurizing characteristics, and 3) low cost.

II. Background

For many typical rocket liquid propellants, the fluid dynamics of the propellant feed system and injectors are relatively straightforward, and propellants like hydrogen peroxide (H_2O_2), nitrogen tetraoxide (N_2O_4), ethanol (C_2H_5OH), and RP-1 ($C_{12}H_{24}$) are all modeled accurately with incompressible fluid assumptions. Similarly, gaseous propellants like gaseous oxygen (O_2), hydrogen (H_2), and methane (CH_4) are all fairly well modeled, using the ideal gas law and associated compressible fluid relationships. Even liquid oxygen (LOX), which is technically in a saturated state at cryogenic temperatures, is accurately modeled by single-phase incompressible flow. The compressibility factor Z of LOX at 1 atm pressure is 0.004, and the Z factor for saturated cryogenic oxygen vapor is 0.97, very close to the ideal values of 0.0 and 1.0 [1].

A. Two-Phase Flows

Conversely, N_2O has a room-temperature liquid Z factor of 0.13 and a saturated-vapor compressibility Z factor of 0.53. These properties of N_2O make the incompressible liquid and ideal gas assumptions highly inaccurate for quantitative analytical models. Also, because normal operating temperatures for N_2O are near the critical point of the fluid, N_2O cannot be assumed to be solely a gas or liquid, but it must be treated as a two-phase mixture. Two-phase flows involve the combined flow of a liquid phase and a gas or vapor phase. In a given sample of fluid, the ratio of the mass of the vapor divided by the total fluid mass is referred to as the fluid quality. With self-pressurizing systems using saturated liquids, as the tank evacuates, liquid boils into vapor, and the fluid quality continually changes. This constantly changing vapor fraction produces large variations in the internal tank pressure and effective fluid density. The fluid pressure and density are key factors that determine the injector mass-flow rate and the resulting combustion mixture ratio, chamber pressure, combustion stability, and thrust evolution. Clearly, understanding and modeling these fluid properties across the tank/injector outlet are critical for predicting the overall rocket performance.

B. Two-Phase Extensions to the Ideal Gas Equation

Modeling compressible saturated fluids requires extensions to the traditional real gas equation of state. In cases in which the ideal gas assumption is not acceptable, the gas phase can be modeled with a cubic equation, like the van der Waals model [2]. The van der Waals equation is the oldest extension to the ideal gas equation. It is significantly more accurate than the ideal gas law and can be used to roughly predict when a gas will condense. It is often used as a first-order approach to correcting for nonideal gas effects. This model is numerically well behaved and captures many of the qualitative deviations from ideal gas behavior, but it is poor at describing saturated liquid properties, especially near the critical point. As mentioned earlier, because normal operating temperatures for N_2O are near the critical point, this inaccuracy represents a significant shortcoming of the van der Waals model.

One of the more modern equations-of-state models is the Peng–Robinson model [3], which is most useful for describing nonpolar molecules, such as hydrocarbons or gaseous nitrogen. The model is derived by modifying the attraction pressure term of van der Waals equation. Unlike the van der Waals equation, the Peng–Robinson equation does not use constant parameters, but it allows the attraction pressure parameter to vary as a function of the operating temperature of the fluid. Unfortunately, this model is not very accurate when applied to polarized nonhydrocarbon molecules like N_2O. To address these shortcomings, very accurate (and very complex) multiparameter equations of state have been developed for fluids in which real gas and compressible liquid effects become important [4,5]. The 12-parameter formulation adopted by the National Institute of Standards and Technology (NIST) [6], has been used to develop an extensive database of the thermochemical properties for many common industrial fluids and propellants. This database is available online [7].

C. Saturation Properties for N_2O

Fortunately, N_2O is one of the propellants for which an extensive NIST database exists. Numerical values for N_2O, parsed from this NIST database [7], will be exploited in the model development presented in this paper. These data are used in a black box manner, in which the tables are interpolated as needed without resorting to the complex semiempirical models developed for NIST. Nitrous oxide is a colorless and odorless fluid with a critical saturation temperature of 36.37°C, a critical saturation pressure of 724.5 kPa, and a very high vapor pressure at room temperature of 565 kPa at 25°C. Nitrous oxide is a relatively strong oxidizer with a positive heat of formation. This property makes N_2O both an oxygen contributor and a direct energy contributor in a combustion system.

Figure 1 shows the saturation properties of N_2O, parsed from the NIST database [7], in the traditional form, with the fluid temperature as the independent variable. Figure 1a plots the vapor pressure. There is only one curve here, because the saturated liquid and vapor are at the same pressure. Notice that the vapor pressure varies significantly over the normal operating temperature for N_2O, and a significant temperature drop produces a similar significant pressure drop. Data plotted in Figs. 1b–1d display density, specific entropy, and compressibility as a function of fluid temperature. There are two curves plotted in each of these figures: one for the vapor phase and one for the liquid phase. Also notice that, near room temperature (290 K), Fig. 1d shows that liquid and gaseous compressibility factors deviate significantly from their ideal incompressible fluid or real gas values. These data support the earlier assertions with regard to the significantly nonideal behavior of N_2O.

The data, as plotted in Fig. 1, will now be rearranged to a more convenient form for later use in developing the tank-evacuation model. Here, the NIST tables are rearranged with fluid temperature T, pressure p, and quality χ as dependent variables and effective fluid density ρ and effective specific entropy s expressed as pseudo-independent variables. This unconventional rearrangement is performed to allow convenient calculation of the normal fluid thermodynamic state properties, T, p, and χ, from entropy and density values calculated using the adiabatic expansion model, to be derived in the next section. This transformation is facilitated by first noticing that, when a specific entropy is plotted as a function of density for both the vapor and liquid phases of saturated N_2O, a single continuous monotonic curve is formed with the vapor and liquid curves, meeting in the middle at the critical point. Figure 2 plots these data. The data behavior displayed in Fig. 2 allows the fluid quality to be plotted as a function of the total (two-phase) fluid specific entropy and density. The effective fluid specific entropy for a given vapor mass fraction is

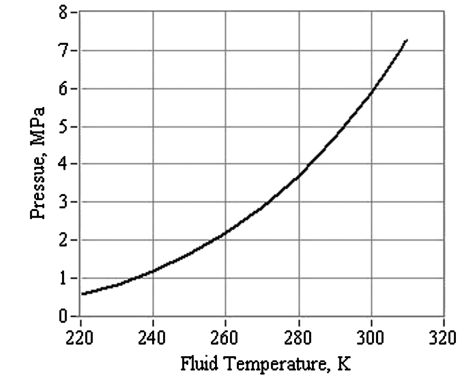

a) Saturation pressure

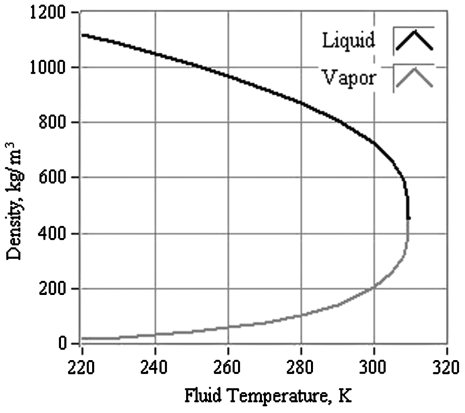

b) Density

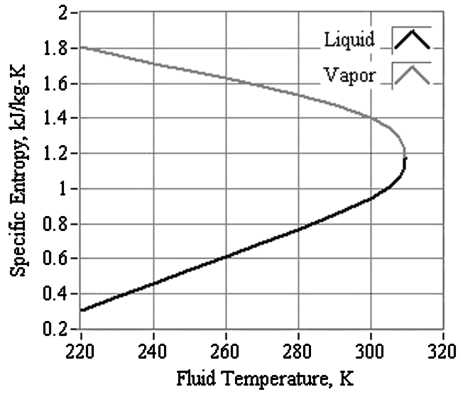

c) Specific entropy

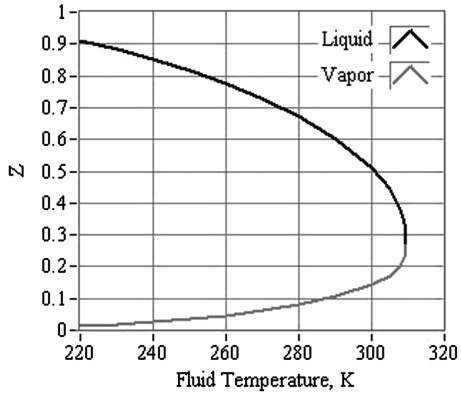

d) Compressibility factor

Fig. 1 Nitrous-oxide saturation properties plotted with temperature as independent variable.

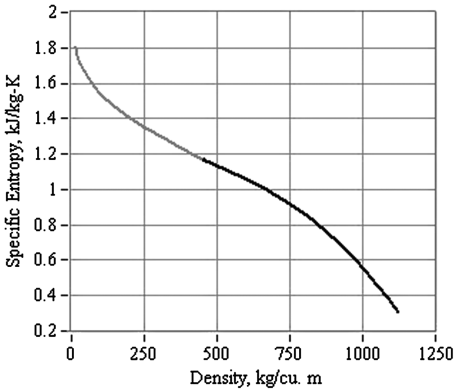

Fig. 2 Specific entropy characteristic relationship with fluid density.

$$s = \frac{s_L \cdot m_L + s_V \cdot m_V}{m_L + m_V} = s_L \frac{m_L}{m_L + m_V} + s_V \frac{m_V}{m_L + m_V}$$
$$= s_L \cdot (1 - \chi) + s_V \cdot \chi \tag{1}$$

In a similar manner, the effective fluid density in the tank is

$$\rho = \frac{m_{\text{total}}}{V_{\text{tank}}} = \frac{m_L + m_V}{V_{\text{tank}}} = \frac{m_L + m_V}{V_L + V_V} = \frac{\rho_V . \rho_L}{\rho_L \chi + \rho_V (1 - \chi)} \tag{2}$$

In Eqs. (1) and (2), the subscripts V and L refer to the vapor and liquid thermodynamic states, respectively, m is the fluid mass quantity, V_{tank} is the internal volume of the propellant tank, and V_L and V_v are the tank volumes occupied by liquid and vapor, respectively. Using the relationships of Eqs. (1) and (2) and the data plotted in Figs. 1c and 2, the saturated N_2O database is parsed using a nonlinear solver, and the fluid quality is plotted as a dependent variable, with total fluid density and total specific entropy as independent variables. Figure 3 displays this result. Figure 3a shows the relationship of fluid quality to the specific entropy and density. Figures 3b–3d present similar relationships for fluid temperature, pressure, and specific enthalpy. Only the saturated fluid properties are plotted in these graphs.

It is acknowledged that the presented fluid property plots (Figs. 3a–3d) have a limited breakpoint density distribution with regard to specific entropy as an independent variable. This lack of density is necessary in order to make the individual lots viewable. In the actual interpolation scheme, the density of the specific entropy break points is actually two orders of magnitude greater than displayed. Both linear interpolation and cubic-spline-interpolation routines yield identical lookup results for the actual numerical schemes.

Although the resulting fluid quality and specific entropy curves are nonmonotonic, they are all continuous and have no singularities. These features allow the database to be efficiently parsed using conventional interpolation and approximation techniques [8]. A variety of methods, including linear interpolation and cubic spline fits, were evaluated. Both methods produced similar results. In the end, linear interpolation of densely packed property tables was used for the real-time algorithm. A numerical uncertainty analysis shows that the root-mean-square errors between the table interpolations and the NIST models are less than 0.5% across the entire nitrous-oxide saturation dome.

D. Existing Two-Phase Injector Models

In a typical constant-pressure injector design, the propellants are generally assumed to be quasi-incompressible liquids, and the incompressible discharge coefficient equation [9]

$$\frac{\dot{m}_{\text{inc}}}{A_c} = C_d \sqrt{2\rho_1 (P_1 - P_2)} \tag{3}$$

predicts mass flux very accurately when the injector or orifice discharge coefficient C_d is well characterized. In Eq. (3), $\dot{m}_{\text{inc}}$ is the

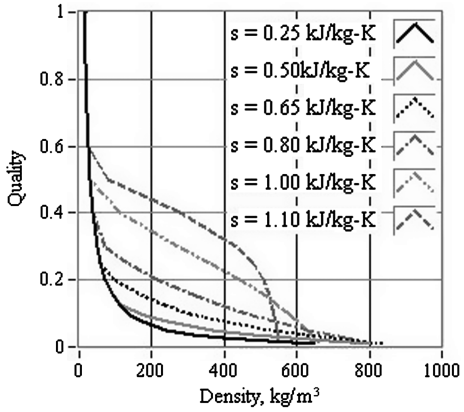

a) Fluid quality/density

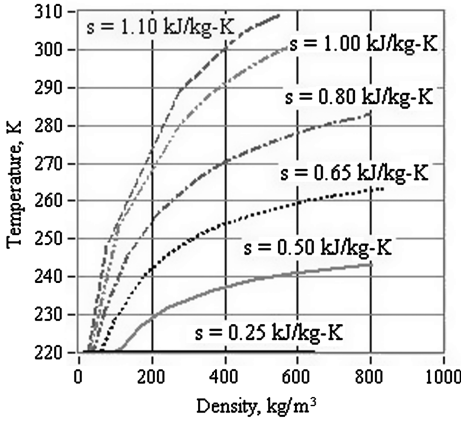

b) Temperature/density

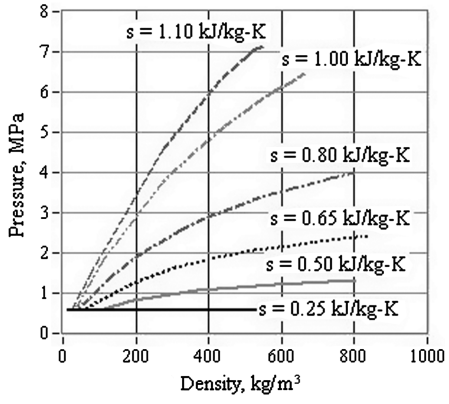

c) Pressure/density

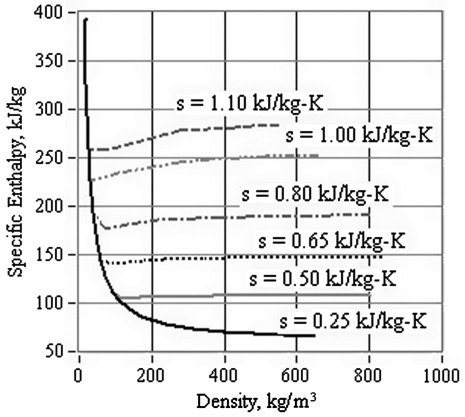

d) Specific enthalpy/density

Fig. 3 Reorganized nitrous-oxide saturation properties plotted with entropy and density as pseudoindependent variables.

incompressible mass-flow rate, A_c is the port cross-sectional area, P_1 is the upstream pressure, and P_2 is the downstream pressure. This model assumes that the flow through the orifice is single phase and that variations in density are negligible. Viscous losses in the orifice are accounted for in the empirically determined discharge coefficient.

1. Homogeneous Equilibrium Model

With self-pressurizing propellants, like N_2O, the fluid static pressure is often very close to the saturation pressure, and flow losses cause the exit pressure to drop well below the saturation pressure when flowing across the injector port. These local static pressure drops result in vapor cavitation and can choke the flow in the injector port, limiting the available mass flow. If the liquid and vapor phases are assumed to be in phase equilibrium, there is no velocity difference (no slip) between the liquid and gaseous phases. This flow condition is referred to as homogeneous equilibrium. When the no-slip fluid equilibrium assumption is applied, and if the expansion process is assumed isentropic (no entropy growth), Leung [10] shows that the injector mass flux can be written in terms of the fluid enthalpy drop across the port. This mass-flux model is referred to as the homogeneous equilibrium model (HEM) [11]. The HEM mass flux is described by

$$\frac{\dot{m}_{\mathrm{HEM}}}{A_c} = C_d \cdot \rho_2 \sqrt{2(h_1 - h_2)} \tag{4}$$

In Eq. (4), $\dot{m}_{\mathrm{HEM}}$ is the homogeneous equilibrium mass-flow rate, ρ_2 is the total two-phase fluid density downstream of the injector port, h_1 is the upstream specific enthalpy, and h_2 is the downstream specific enthalpy. For a given upstream pressure, when P_2 is gradually lowered, the HEM predicts a critical pressure ratio across the outlet, where the mass flux reaches a maximum value.

Figure 4 presents an example of a calculation in which predicted outlet mass flux and fluid quality downstream of the outlet orifice are presented as a function of the orifice pressure ratio for four different tank-fluid temperatures. For this calculation, the upstream fluid is assumed to be saturated, and the fluid escaping the tank is entirely liquid ($\chi = 0$) on the upstream side of the outlet. The assumed discharge coefficient is $C_d = 0.8$. This value for discharge coefficient is used for consistency, with the empirically determined outlet discharge coefficient for data to be presented later in Sec. IV.

In all of the presented cases, the critical pressure ratio for which the mass flow reaches a maximum lies between 0.7 and 0.8. For comparison purposes, Fig. 4c plots the mass flux predicted by Eq. (3): the incompressible discharge coefficient formula. Clearly, the traditional incompressible formula does not limit the mass flux to a maximum value for higher orifice pressure ratios.

Experimental results for low-aspect-ratio (ratio of length to diameter L/D) orifices show that HEM-predicted mass flows are significantly lower than actually occur, and they tend to favor the incompressible model of Eq. (3) [1]. Although some investigators have speculated that flow slip between the vapor and liquid phases causes this effect [12], this discrepancy is likely due to a finite rate of mass transfer between the liquid and vapor phases. This nonequilibrium effect does not allow for the flow to reach thermodynamic equilibrium for a short-run length [1]. Clearly, for low-aspect-ratio ports, the limiting mass flux occurs considerably later than predicted by the HEM.

2. Homogeneous Nonequilibrium Model

With regard to this predicted mass flux for the HEM, [13] shows that the measured mass flux approaches the values predicted by the HEM as the aspect ratio L/D increases. This nonequilibrium effect is more pronounced as the incoming pressure rises. The homogeneous nonequilibrium model (HNE) [13] was developed to account for this observed rate of mass transfer by assuming that vaporization is not complete until the fluid has traveled some minimum distance along the flow path. The HNE model accounts for nonequilibrium effects by creating a nonequilibrium multiplier to scale the predicted rate of

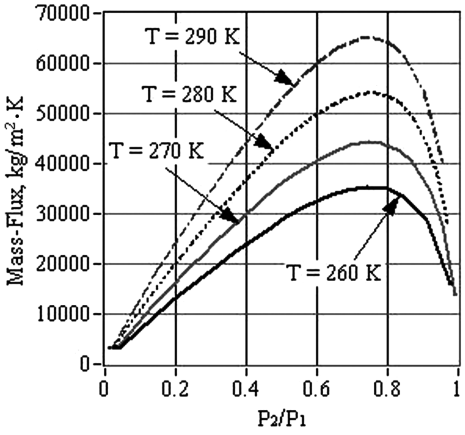

a) HEM, Mass-Flux

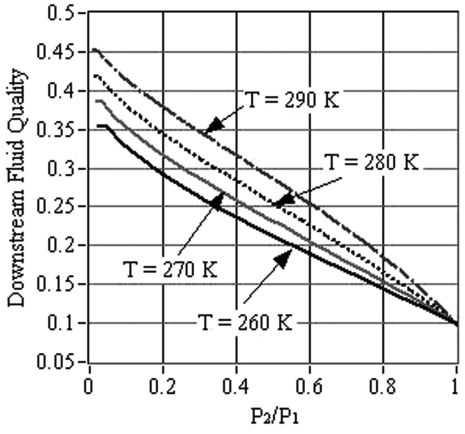

b) HEM Downstream Fluid Quality

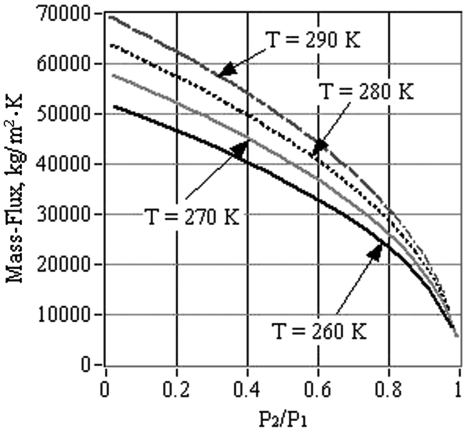

c) Discharge Coefficient Formula, Mass-Flux

Fig. 4 Effect of outlet-pressure ratio on mass flux and downstream fluid quality.

vapor–liquid mass transfer, so that the HNE model converges on the HEM model as the run length increases. This approach is conceptually sensible, as the flow has longer to obtain full equilibrium as the length of a tube increases. When compared with the HEM, the HNE model results in a higher overall mass flux. In general, this model works well for most fluids and for longer tubelike flowpaths; but is not readily applicable to simple orifices with low aspect ratios. Also, the developed correlation for the scale factor does not perform well when compared with nitrous-oxide injector data. Typically, the HNE model overpredicts the mass flux by a significant amount for nitrous oxide [1].

3. Nonhomogeneous Nonequilibrium Model

To overcome these modeling shortcomings, Dyer et al. [1] have proposed a model that blends the HEM and incompressible [Eq. (3)] models. This nonhomogeneous nonequilibrium (NHNE) model reasons that the longer the fluid remains within the injector element, the longer it has for the fluid to vaporize and reach equilibrium homogeneity. The degree of vaporization that occurs depends on the rate of bubble growth [14] when compared with the dwell time within the port. They propose a modified form of the cavitation number that is proportional to the ratio of the vapor-bubble-formation time to the port-dwell time. The NHNE weighting parameter κ is given as a function of the orifice inlet P_1, the outlet pressures P_2, and the vapor pressure P_v of the fluid at the outlet temperature:

$$\kappa = \sqrt{\frac{P_1 - P_2}{P_v - P_2}} \tag{5}$$

Reasoning that the mass flux should vary smoothly between the predicted incompressible and HEM mass-flux values, the NHNE model is defined as the weighted average of the two models:

$$\frac{\dot{m}_{\mathrm{NHNM}}}{A_c} = \frac{(\dot{m}_{\mathrm{inc}}/A_c) + \kappa(\dot{m}_{\mathrm{HEM}}/A_c)}{1 + \kappa} \tag{6}$$

Experimental data collected by [1], from over 100 hot fires of nitrous-oxide hybrid motors with mass flows up to 0.6 kg/s, demonstrate that this model does a good job of predicting the injector mass flux as long as the upstream fluid properties are well characterized. The model predicts mass flows to within 15% in all cases, with an overall experimental standard deviation of 98.5%. Figure 5 presents the predicted mass flux from the NHNE model, using the previously described conditions for the data of Fig. 3. The model still shows a mass-flux limiting effect at injector pressure ratios below 0.60, but it now allows considerably higher mass fluxes for large injector pressure drops.

III. Adiabatic Two-Phase Entropy Model Development

Development of the complete engineering model for the N_2O tank evacuation is presented in this section. The entropy-based model builds on the NHNE model of Eq. (6) and overcomes the mass-flow inaccuracies for both the HEM and NHE models, as described in the previous section. As the tank evacuates, the total entropy in the tank decreases (as mass leaves the tank) but, at any time, the sum of the entropy in the tank and the entropy evacuated from the tank equates to the initial total fluid entropy in the tank. Thus, with regard to the entire process, the flow is isentropic, but with regard to the propellant tank control volume, the process is nonisentropic. The isentropic assumption for the expansion process is not significantly different than the isentropic flow assumption used to develop the one-dimensional

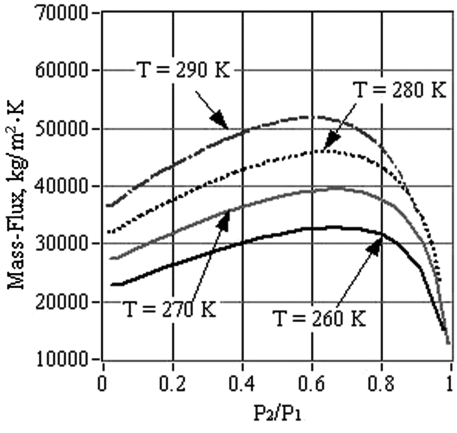

Fig. 5 NHNE mass-flux predictions.

De Laval flow equations used to model the performance of rocket nozzles [15]. Effectively, the overall entropy increase for the process is small when compared with the initial tank entropy and the entropy exported from the tank. Data presented later in this paper demonstrate that, at least for N_2O as a working fluid, the isentropic assumption provides a mechanism by which the critical parameters of tank pressure, tank temperature, and exit mass flow can be accurately predicted.

Other less-significant assumptions used for developing this model are as follows:

1) The tank is small enough, so that the pressure equalizes instantly within the entire internal tank volume during evacuation.

2) No external heat transfer to the fluid occurs during the evacuation process.

3) The fluid in the tank is stratified with distinct liquid and vapor layers.

4) The fluid hydrostatic pressure is negligible when compared with the saturation vapor pressure.

5) The fluid flashes to vapor downstream of the tank outlet and is either entirely liquid or entirely vapor as it enters the tank outlet.

The latter circumstance (vapor only) is allowed to account for the point at which all liquid has been drained from the tank. An allowance for a vapor vent at the top of the tank will be included in the model. Figure 6 depicts this tank model. As the liquid escapes through the outlet, fluid boils off to create additional vapor that occupies the volume at the top of the tank. Some of the vapor simultaneously condenses near the liquid interface.

A. Initial Conditions

Given the initial temperature and pressure of the saturated propellant in the tank, T_0 and P_0, the initial densities of the saturated liquid and vapor phases, ρ_L and ρ_V, are calculated by interpolation of the NIST saturation property charts in Fig. 1b. Because the volume of the propellant tank and the initial propellant mass are known constants, the initial fluid quality within the tank can be calculated as

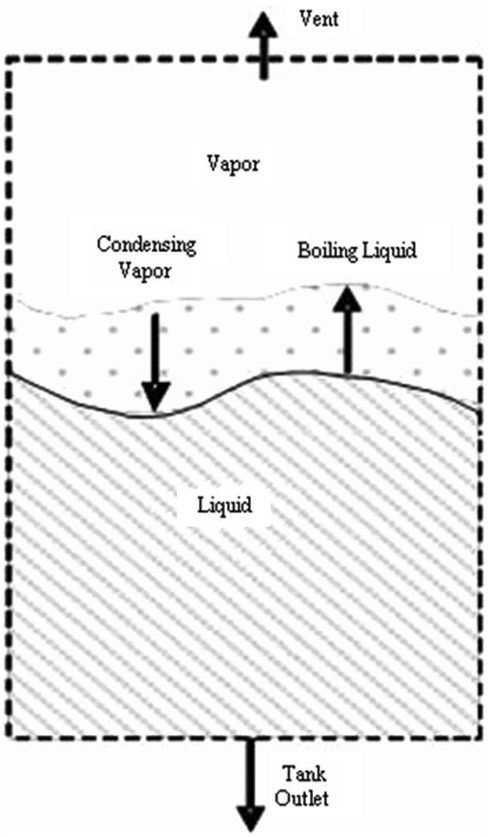

Fig. 6 Schematic of stratified tank model showing vent and outlet.

$$\chi = \frac{\rho_V.\rho_L - \rho_V \cdot \rho_0}{\rho_0(\rho_L - \rho_V)} = \frac{(\rho_V.\rho_L) - \rho_V \cdot (m_0/V_{\text{tank}})}{(m_0/V_{\text{tank}})(\rho_L - \rho_V)} = \frac{(\rho_V.\rho_L)V_{\text{tank}} - \rho_V \cdot m_0}{m_0(\rho_L - \rho_V)} \tag{7}$$

Using the calculated value for χ, and the s_v and s_L (looked up from Fig. 1c), the initial effective specific entropy s_0 is calculated using Eq. (1). At the beginning of the tank evacuation, the total entropy S_0 stored in the tank is calculated by multiplying the initial effective specific entropy by the initial fluid mass in the tank:

$$S_0 = m_0 \cdot s_0 \tag{8}$$

As described earlier, when the tank begins to evacuate, the total entropy in the tank decreases (as mass leaves the tank) but, at any time, the sum of the entropy in the tank and the entropy evacuated from the tank equates to the initial total entropy given by Eq. (8).

B. Two-Phase Propagation Algorithm

With the initial conditions now specified, the time history for the propellant properties in the tank can be found for the entire blow down. As pictured in Fig. 6, the particular tank being modeled (and tested in this project) includes a top vent that continuously vents vapor, ensuring that overpressurization does not occur during the motor firing. The vent valve also allows for a higher fill level in the propellant tank. Both the liquid propellant escaping from the tank outlet and the vapor propellant escaping from the vent are modeled. The liquid mass flow escaping from the lower tank outlet $\dot{m}_{L,\text{out}}$ is modeled using the NHNE model described earlier. This relationship can be expressed in terms of the tank and outlet conditions as

$$\dot{m}_{L,\text{out}} = A_{\text{out}} \cdot \frac{(\dot{m}_{\text{inc}}/A_c) + \kappa(\dot{m}_{\text{HEM}}/A_c)}{1+\kappa} = (A_{\text{out}} \cdot C_{d\text{out}}) \cdot \frac{[\sqrt{2\rho_L(P_{\text{tank}} - P_{\text{out}})(P_v - P_{\text{out}})} + \rho_2\sqrt{2(P_{\text{tank}} - P_{\text{out}})(h_{\text{tank}} - h_{\text{out}})}]}{\sqrt{P_v - P_{\text{out}}} + \sqrt{P_{\text{tank}} - P_{\text{out}}}} \tag{9}$$

Vapor mass flow out of the top vent $\dot{m}_{\text{vent}}$ is calculated by

$$\dot{m}_{\text{vent}} = (A_{\text{vent}} \cdot C_{d_{\text{vent}}}) \cdot \sqrt{\gamma P_{\text{tank}} \cdot \rho_V \left(\frac{2}{\gamma+1}\right)^{(\gamma+1)/(\gamma-1)}} \tag{10}$$

In Eqs. (9) and (10), $C_{d\text{out}}$ and $C_{d\text{vent}}$ are the discharge coefficients for the tank-outlet orifice and the vapor vent, A_{out} and A_{vent} are the exit areas of the tank outlet orifice and vapor vent, P_{tank} is the vapor pressure in the tank, γ is the ratio of specific heats for the vapor thermodynamic state, and P_{out} is the pressure to which the tank outlet is dumping. P_v is the vapor pressure at the tank-outlet temperature. Equation (9) assumes that the vapor pressure in the tank is sufficient to insure that the outlet fluid is liquid and only flashes to vapor after entering the injector port. Equation (10) is the compressible form of the discharge coefficient equation for choked flow [9]. Equation (10) assumes that, during two-phase flow, the internal vapor pressure in the tank will always be sufficiently large to choke the vapor flow through the top vent.

During the tank evacuation, the total change of mass within the tank equals the mass of liquid that is expelled from the tank orifice and the mass of vapor vented off the top of the tank. The new total tank entropy is the total entropy from the previous step, decremented by the entropy that leaves the tank control volume with the exiting vent and outlet mass flow:

$$S_{i+1} = S_i - (m_{L,\text{out}} \cdot s_L)_i - (m_{\text{vent}} \cdot s_V)_i \tag{11}$$

In Eq. (11), the subscript i is the discrete time index, and the time interval between indices is Δt. In Eq. (10), $m_{L,\text{out}}$ is the liquid mass that escapes through the tank-outlet valve, and m_{vent} is the vapor mass that escapes through the top vent. These mass values are calculated by numerically integrating Eqs. (9) and (10):

$$m_{i+1} = m_0 - \int_0^t \dot{m}_{L,\text{out}}\,\mathrm{d}t - \int_0^t m_{\text{vent}}\,\mathrm{d}t$$
$$\approx m_i - (\dot{m}_{L,\text{out}} + \dot{m}_{\text{vent}}) \cdot \Delta t \tag{12}$$

The new effective tank-specific entropy is calculated using the mass and total entropy from the current step,

$$s_{i+1} = \frac{S_{i+1}}{m_{i+1}} \tag{13}$$

and the updated effective density is calculated by

$$\rho_{i+1} = \frac{m_{i+1}}{V_{\text{tank}}} \tag{14}$$

The updated density and specific entropy values are now used to calculate the new temperature, pressure, and fluid quality in the tank, using a table lookup on the data in the NIST property tables described earlier in the paper. The remaining liquid and vapor masses in the tank are calculated as

$$\begin{bmatrix} m_V = \chi \cdot m_{i+1} \\ m_L = (1-\chi) \cdot m_{i+1} \end{bmatrix} \tag{15}$$

Equations (9–15), along with the saturation properties of Figs. 1–3, collectively make up the engineering model that describes the tank-evacuation process. These equations are numerically integrated over time (and the database is parsed) to continuously calculate the tank-fluid state properties as a function of time. This model intrinsically takes into account the masses of liquid and vapor that change phase due to boiling and condensation. The model also allows for some fraction of two-phase flow through the lower-tank-outlet port.

C. Vapor-Phase Propagation Algorithm

As described earlier, the fluid in the tank is assumed to be stratified, with vapor at the top of the tank and liquid at the bottom. With the outlet on the bottom of the tank, initially, all of the fluid leaving the tank is saturated liquid. As fluid mass leaves the tank, liquid in the bottom of the tank boils, producing vapor to fill the tank void. Eventually, all of the liquid is consumed, and only saturated vapor exits the tank. This event will be indicated when the internal tank-fluid quality approaches 1.0. At this point, the NHNE model does not apply for the tank outlet, because only saturated vapor remains within the tank volume. In this circumstance, only data for saturated vapor are applicable, and the tank outlet mass flow is calculated using the choked-flow compressible version of the discharge coefficient equation:

$$\dot{m}_{V,\text{out}} = A_{\text{out}} C_{d_{\text{out}}} \cdot \sqrt{\gamma P_{\text{tank}} \cdot \rho_V \left(\frac{2}{\gamma+1}\right)^{(\gamma+1)/(\gamma-1)}} \tag{16}$$

In Eq. (16), the term $\dot{m}_{V,\text{out}}$ indicates that all of the mass leaving the outlet is entirely in vapor form. Near the end of the evacuation, tank pressure drops sufficiently so that, depending on the pressure ratios across the respective orifices, both the vent and outlet flows will no longer remain choked. In this case, the choked compressible discharge coefficient equation is replaced by the subsonic version [9]:

$$\dot{m}_{v,\text{out}} = A \cdot C_d \sqrt{\frac{2\gamma}{\gamma-1}\rho_v P_{\text{tank}} \left[\left(\frac{P_2}{P_{\text{tank}}}\right)^{2/\gamma} - \left(\frac{P_2}{P_{\text{tank}}}\right)^{(\gamma+1)/\gamma}\right]} \tag{17}$$

Here, P_2 is the pressure being evacuated to: ambient for the top vent or chamber pressure at the tank outlet.

IV. Results and Discussion

Results of cold-flow tank-evacuation tests are compared with the engineering model predictions in this section. Using cold-flow measurements allows verification of the propellant evacuation model without the complexity of modeling the entire hybrid combustion process. Whitmore et al. [16] present models and data for hot-flow hybrid configurations. An existing legacy jet-engine test cell was adapted to accommodate all testing for this project. The test cell has 13.5 m^2 of available work space and is fully instrumented. The facility is capable of testing rocket motors with thrust levels up to 22 kN (5000 lb). The legacy test cell is open to ambient air temperature and pressure.

A. Test Hardware Description

The hardware for these characterization tests was derived from a modified commercially available hybrid rocket motor, the Contrail Rockets L-800.[‡] Multiple static hot-fire and cold-flow tests have been performed with this motor. The Contrail Rockets motor uses nitrous oxide (oxidizer) and aluminized hydroxyl-terminated polybutadiene (fuel) as propellants. The system consists of an oxidizer tank in line with a fuel-grain cartridge. The motor is self-pressurized, using the saturation pressure of N_2O to propel oxidizer across a five-port injector. The fuel port lies downstream of this injector face. Each injector port has a diameter of 0.3175 cm, and the total outlet flow area is 0.396 cm^2. The Contrail Rockets L-800 oxidizer tank also features a top vent with a diameter of 0.3175 cm. For these tests, discharge coefficients for each of the injector and vent ports are assumed to have nominal values for short sharp-edged orifices, approximately 0.8 [17]. Figure 7 shows the injector face with the five outlet ports clearly visible. The location of the vent port is shown in Fig. 8.

The evacuation tests were performed using only the oxidizer-tank portion of the hybrid motor without the solid fuel-grain cartridge. Because the test cell was open to ambient conditions, the N_2O feed to the oxidizer tank was thermally maintained at 25°C by storing the supply tank in a heated, thermally insulated chamber to reduce the effects of outside temperature variability on the initial fluid density. Operating at these temperatures, N_2O has a high vapor pressure (approximately 5500 kPa) and allows the oxidizer tank to be almost completely filled.

To measure the mass of the oxidizer leaving the outlet, the tank was suspended with cables from a load cell. A 90 deg elbow was attached to the bottom end of the oxidizer tank to change the direction of the venting gasses, so that the produced thrust would not interfere with the mass measurements. Because the escaping gas produces a force perpendicular to the suspended tank, a loose centering ring was placed on the tank. This ring did not interfere with the vertical force measurements, but it kept the tank from moving laterally. Figure 8 presents a schematic of the test apparatus.

B. Test Instrumentation Description

The evacuation tests were instrumented to measure ambient temperature and pressure, propellant tank pressure and temperature, and propellant mass flow. An Omega LCAE-10kg load cell measured the mass of the propellant tank during the evacuation. Calibration of the load cell was performed at the beginning of each test by taking zero values, while the propellant tank was not suspended from the load cell, and then taking values with an empty propellant tank. The unamplified load-cell output was 3 mV/V for a full-scale range. The manufacturer's specified 3–σ accuracy was 0.5% of the full-scale reading, approximately $\pm$0.5 N. Load-cell readings were filtered posttest to eliminate noise caused by stand vibrations and other miscellaneous noise sources.

A type K thermocouple (TC) was used to measure the temperature of the oxidizer in the tank. This TC was inserted inside the tank and into the fluid, using a thin piece of metal tubing. This placement at the bottom of the tank allowed an accurate fast-response measurement of the liquid temperature to be obtained. The combined TC and reference junction (built into connector block) uncertainties resulted in an estimated end-to-end temperature measurement uncertainty of

[‡]Data available online at http://www.contrailrockets.com/products.htm [retrieved 20 February 2010].

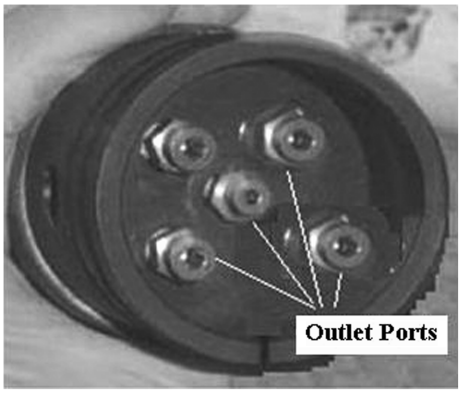

Fig. 7 Contrail L-800 hybrid motor injector face showing outlet ports.

±2.2°C. A Measurement Specialties, Inc. 0–6890 kPa · gauge (0–1000 psig) pressure transducer was used to measure the internal pressure in the oxidizer tank. This pressure transducer has a specified uncertainty of ±0.25% (full scale), which includes linearity, hysteresis, and repeatability. All data were sensed at a rate of 50 samples per second using a National Instruments 16-bit PCMCIA (personal-computer-memory/Card-International-Association) card inserted into a laptop computer.

C. Comparison of Tests Results with Engineering Model Simulation

Figure 9 presents the results from a typical evacuation test. Here, the measured mass, mass-flow, pressure, and temperature profiles are compared with the evacuation model described in Sec. II. Figure 9a compares the predicted vapor and the total mass-flow rates against the measured data. The measured mass-flow rate is calculated by numerically differentiating the load-cell reading. The predicted tank pressure and temperature are compared with the measured values in Figs. 9b and 9c. Finally, Fig. 9d graphs the modeled time histories for the initial total system entropy, the entropy exported from the tank, the residual fluid entropy in the tank, and the specific entropy of the fluid remaining in the tank.

The presented data are typical of all results obtained from the cold-flow tests, and they exhibit a number of important features that are critical in the interpretation of the test results. For this test, the oxidizer tank was filled and then allowed to exhaust through the

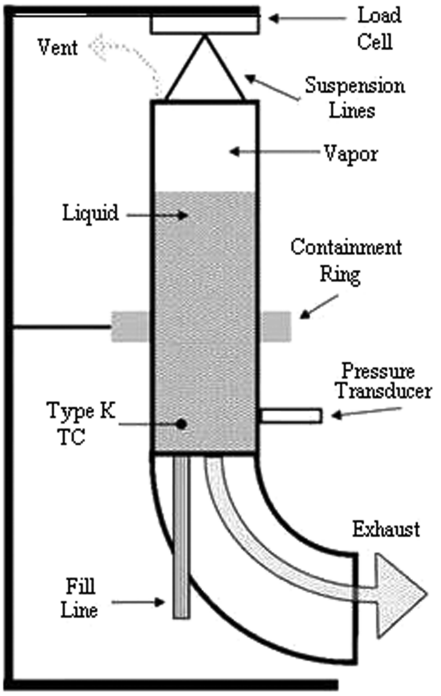

Fig. 8 Schematic of test apparatus for cold-flow tests.

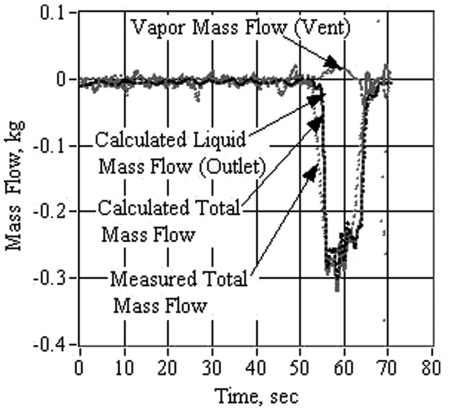

a) Mass-Flow from Tank

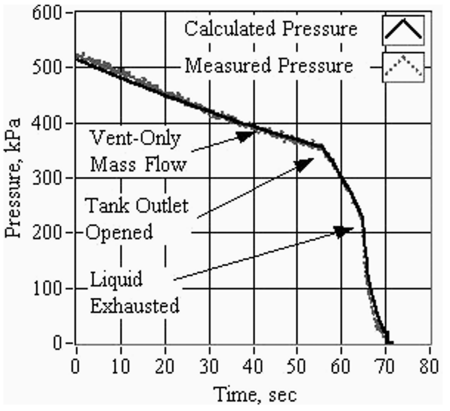

b) Tank Pressure

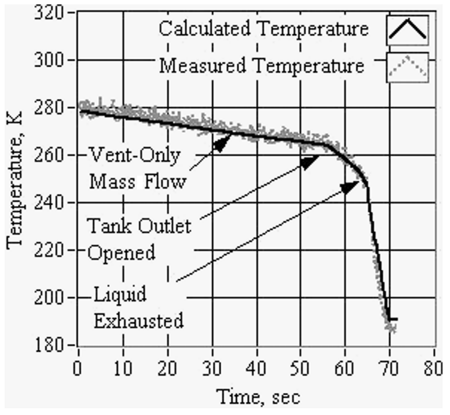

c) Fluid Temperature in Tank

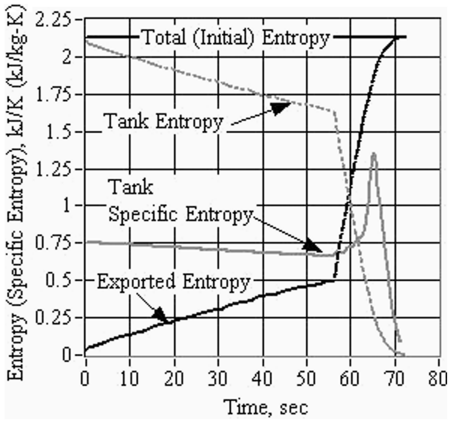

d) Entropy/Specific Entropy

Fig. 9 Model predictions compared with measured results from a typical cold-flow evacuation test.

upper vent port, slightly less than 1 min. before the main outlet port was opened. During this vent period, only gaseous oxidizer left the tank, and the remaining liquid oxidizer was boiled to maintain saturation equilibrium. This slow boil off gradually lowered the pressure and temperature in the tank. The entropy in the tank also decreased gradually. After this venting period, the main tank-exit port was opened, and liquid oxidizer flowed through larger injectors. Simultaneously, vapor was leaving through the upper tank vent. At 65 s, the liquid oxidizer had all been exhausted, leaving only vapor in the tank. From that point on, the internal tank quality was 1.0, and the outlet mass flow was modeled using Eq. (16). Eventually, the tank vapor pressure dropped to the point at which the exit flows no longer choked, and Eq. (17) was used to calculate mass flow. The specific entropy in the oxidizer tank decreased throughout the venting process, and then it increased once the tank exit was opened, and the liquid was allowed to leave the tank. Once all of the liquid was expelled, the specific entropy once again decreased. The breaks when the liquid began to vent and when all of the liquid had been expelled were clearly visible. These events are labeled in Figs. 9c and 9d.

Because the predicted total tank mass and total mass-flow data show such good agreement with the measured data for venting, fluid evacuation, and vapor evacuation phases of the blow down, one can conclude that the NHNE model does a very good job of modeling the outlet mass flow, and the entropy-tracking procedure does a good job of predicting the saturation temperature and pressure in the tank. For the short duration of this test run, the adiabatic process assumption appears to be completely valid.

V. Conclusions

Self-pressurizing propellant feed systems, due to their overall simplicity, offer attractive options for propulsion system designers. These systems inherently exhibit transient properties as the tank-fluid mass bleeds down, and modeling the two-phase evacuation process using CFD presents an extremely complex and time-intensive problem. As an alternative, a simple engineering model was developed for self-pressurized propellant feed systems, using saturated compressible propellants. Key assumptions here were 1) the tank was small enough, so that pressure equalized instantly within the internal tank volume, 2) no external heat transfer to the fluid, 3) fluid in the tank was stratified with distinct liquid and vapor layers, 4) fluid hydrostatic pressure was negligible when compared with the saturation vapor pressure, and 5) fluid flashed to vapor downstream of the tank outlet and was either entirely liquid or entirely vapor as it entered the tank outlet. During evacuation, the sum of the fluid entropy in the tank and the fluid entropy that had escaped through the feed system equaled the total initial entropy of the tank fluid. The evacuated entropy was subtracted from the total entropy at the thermodynamic state of the fluid, leaving the tank, and the new thermodynamic state with the existing mass and entropy was calculated using two-phase thermodynamic property tables. This procedure allowed the thermodynamic states of the propellant to be computed at every stage of the tank evacuation and intrinsically took into account the masses of liquid and vapor that changed phase due to boiling and condensation.

Comparisons with ground test data show that the evacuation model does a good job of capturing key features, including the point at which the liquid oxidizer has all been exhausted, leaving only vapor in the tank. The specific entropy in the oxidizer tank decreases throughout the venting process, and then it increases once the tank exit is opened, and liquid is allowed to leave the tank. Once all of the liquid is expelled, the specific entropy once again decreases. The breaks when the liquid begins to vent, and when all of the liquid has been expelled, are clearly visible.

The simple entropy-based model developed in this paper has been demonstrated to be very accurate for nitrous-oxide applications. The isentropic assumption for the expansion process is not significantly different than the isentropic flow assumption used to develop the one-dimensional De Laval flow equations used to model the performance of rocket nozzles. Effectively, the overall entropy increase for the process is small when compared with the initial tank entropy and the entropy exported from the tank. The model executes rapidly and is easy to implement. It offers a useful tool and, when used early in the design process, has the potential to cut substantial time from the design cycle. When applied to existing systems, the NHNE mass-flow model overcomes the predicted mass-flow inaccuracies observed for both the HE and HNE models, currently considered to be state of the art for two-phase orifice flows. Although the model is developed using saturation fluid properties for nitrous oxide, it is readily extensible to other saturated propellants.

References

[1] Dyer, J., Doran, E., Dunn, Z., and Lohner, K., "Modeling Feed System Flow Physics for Self-Pressuring Propellants," 43rd AIAA/ASME/SAE/ASEE Joint Propulsion Conference & Exhibit, AIAA Paper 2007-5702, July 2007.

[2] Hill, T. L., *Statistical Thermodynamics*, Addison Wesley Longman, Reading, PA, 1960, pp. 280–282.

[3] Peng, D. Y., and Robinson, D. B., "A New Two-Constant Equation of State," *Industrial and Engineering Chemistry Fundamentals*, Vol. 15, No. 1, 1976, pp. 59–64. doi:10.1021/i160057a011

[4] Span, R., and Wagner, W., "Equations of State for Technical Applications, 2: Results for Nonpolar Fluids," *International Journal of Thermophysics*, Vol. 24, No. 1, Jan. 2003, pp. 41–109. doi:10.1023/A:1022310214958

[5] Span, R., and Wagner, W., "Equations of State for Technical Applications, 3: Results for Polar Fluids," *International Journal of Thermophysics*, Vol. 24, No. 1, Jan. 2003, pp. 111–162. doi:10.1023/A:1022362231796

[6] Lemmon, E. W., and Span, R., "Short Fundamental Equations of State for 20 Industrial Fluids," *Journal of Chemical and Engineering Data*, Vol. 51, No. 3, 2006, pp. 785–850. doi:10.1021/je050186n

[7] "Thermophysical Properties of Fluid Systems," [online database], National Institute of Standards and Technology, http://webbook.nist.gov/chemistry/fluid/ [retrieved 30 March 2010].

[8] Rade, L., and Westergren, B., *Beta Mathematics Handbook*, 2nd ed., CRC Press, Boca Raton, FL, 1990, pp. 331–332.

[9] Anon., "Flow Equations for Sizing Control Valves," American National Standards Institute/Instrument Society of America ANSI/ISA-75.01.02, Research Triangle Park, NC 2002.

[10] Leung, J., "A Generalized Correlation for One-Component Homogeneous Equilibrium Flashing Choked Flow," *AIChE Journal*, Vol. 32, No. 10, Oct. 1986, pp. 1743–1746. doi:10.1002/aic.690321019

[11] Darby, R., "Evaluation of Two-Phase Flow Models for Flashing Flow in Nozzles," *Process Safety Progress*, Vol. 19, No. 1, April 2000, pp. 32–39. doi:10.1002/prs.680190109

[12] Darby, R., Meiller, P. R., and Stockton, J., "Select the Best Model for Two-Phase Relief Sizing," *Chemical Engineering Progress*, Vol. 97, No. 5, May 2001, pp. 56–64.

[13] Henry, R. E., and Fauske, H. K., "The Two-Phase Critical Flow of One-Component Mixtures in Nozzles, Orifices and Short Tubes," *Journal of Heat Transfer*, Vol. 5, No. 25, May 1971, pp. 179–187.

[14] Yuan, W., and Schnerr, G. H., "Numerical Simulation of Two-Phase Flow in Injection Nozzles: Interaction of Cavitation and External Jet Formation," *Journal of Fluids Engineering*, Vol. 125, No. 6, Nov. 2003, pp. 963–969. doi:10.1115/1.1625687

[15] Anderson, John, D., *Modern Compressible Fluid Flow with Historical Perspective*, 3rd ed., McGraw–Hill, Boston, MA, 2003, Chaps. 1, 3, 5.

[16] Whitmore, S. A., Chandler, S., and Eilers, S. D., "Transient Thrust Model for a Small Scale Self-Pressured Hybrid Rocket Motor," 45th AIAA/ASME/SAE/ASEE Joint Propulsion Conference and Exhibit, AIAA Paper 2009-5221, 2009.

[17] Sutton, G. P., and Biblarz, O., *Rocket Propulsion Elements*, 7th ed., Wiley, Hoboken, NJ, 2001, Chap. 6.

K. Frendi
Associate Editor